

# Nano/Microrobots in Action for Gastrointestinal Tract Diseases

Subjects: [Biochemical Research Methods](#) | [Infectious Diseases](#) | [Geriatrics & Gerontology](#)

Contributor: Bahareh Khezri

Nano/microrobots (NMRs) are tiny devices that can convert energy into motion and operate at nano/microscales.<sup>54</sup> Especially in biomedical research, NMRs have received much attention over the past twenty years because of their excellent capabilities and great potential in various applications, including on-demand drug delivery, gene and cell transport, and precise microsurgery. Reports published in recent years show that synthetic nano/microrobots have promising potential to function in the gastrointestinal (GI) region, particularly in terms of drug delivery.

nano/microrobots

biomedical applications

imaging

stomach diseases

micromotors

microswimmers

drug delivery

## 1. Introduction

In 1966, the science fiction 'Fantastic Voyage' <sup>[1]</sup> used an example of a famous speech of Richard Feynman 'There is plenty room at the bottom', delivered in 1959 <sup>[2]</sup>. He talked about smart tiny devices that can be swallowed, swim through blood vessels, and remove damaged parts, and then the movie presents a submarine that is shrunk to the size of a microbe to fix the clot on a mission to rescue a scientist. The idea of using nano/microrobots (NMRs) for biomedical applications was mostly initiated by these two events <sup>[1][2]</sup>. As nanotechnology boundaries have been pushed, scientists and researchers have developed tiny robots and presented many "proof-of-concept" and "preliminary demonstration" studies over the past 20 years.

NMRs made from or coated with functionalized and appropriate materials have the ability to swim using either a chemical fuel presented ideally in the same environment or an external source. Since the first report on rod-shaped Au/Pt nanomotors driven by the hydrogen peroxide catalytic reaction, <sup>[3]</sup> this research field has progressed extensively to achieve nano/microrobots with a sophisticated design capable of performing complex tasks. Different materials have been used to achieve these goals, including polymers <sup>[4][5][6]</sup>, two-dimensional materials <sup>[6][7]</sup>, metal-organic frameworks (MOFs) <sup>[8]</sup>, and hybrid materials <sup>[9]</sup>. In addition, many efforts have been made to use different catalytic reactions <sup>[4][5][6]</sup> or integrate components that respond to an external energy source (magnetic field <sup>[7]</sup>, electrical field <sup>[8]</sup>, acoustic wave <sup>[9]</sup>, and light <sup>[10]</sup>) and allow them to be controlled remotely. Since then, many proof-of-concept studies have been reported in various fields such as biomedical <sup>[11][12]</sup>, environmental <sup>[13]</sup>, defense, and food safety <sup>[14][15]</sup> demonstrating the high potential and feasibility of NMRs in real applications. Their small size and mobility make them promising tools with versatile applications in the biomedical field. For example, in recent decades, localized drug delivery systems have received significant attention due to the high demand for efficient

functionality and a reduction in the side effects of therapy [16]. The challenges of the accompaniment of targeted drugs in clinical practice are the following: (i) finding the target in a specific disease, (ii) finding a drug which can cure/prevent it, and (iii) having a drug carrier capable of reaching the target safely. NMRs have shown that they can function as an active and promising self-propelled platform for drug delivery [17][18][19][20][21]. These tiny robots combine the benefits of traditional carriers such as drug protection, selectivity, and biocompatibility with their ability to swim and penetrate into the targeted tissues and release the drug at the desired time and location. To accomplish the task of NMR-based drug delivery, high power is required to drive the robots, control motion and navigate through the predefined pathways. To achieve efficient pickup, transport, and delivery of drugs, a specific interaction between robots and drugs (e.g., electrostatic and hydrogen bonding) is required. In particular, the latest advances in the architecture and development of motors have led to great achievements in the driving force, manipulated motion, velocity, and functionality of the outer layer of tiny motors [17][18][19][20][21].

*Helicobacter pylori* is considered one of the most common bacterial infections. Studies show that in most cases it is responsible for inflammatory gastritis [22], stomach ulcers [23][24], extragastrointestinal diseases [25][26], and the risk of gastric cancer [27]. The traditional standard treatment of *H. pylori* infection is a three-course therapy that requires the prescription of two antibiotics (clarithromycin and amoxicillin/metronidazole) and a proton pump inhibitor (PPI) [24]. It has been shown that prolonged treatment with multiple broad-spectrum antibiotics and proton pump inhibitors causes other health complications [28]. The reported diseases associated with long-term use of PPIs in the literature are *C. difficile* infection, dementia, pneumonia, antiplatelet agents, kidney disease, micronutrients, and bone mineral density deficiency [28]. Long-term administration of antibiotics also has adverse effects on beneficial bacteria and also resistance to further treatment using the same antibiotics. These adverse side effects of traditional medicine and their nontargeting effects urge us to look for an effective vaccine and alternative therapeutic options [29][30] ([Scheme 1](#)).



**Scheme 1.** Schematic of reported in vivo treatment and imaging of stomach diseases using nano/microrobots. (A) Invented oral medicine based on nano/microrobots for prevention (vaccine) and treatment (tablet) of stomach diseases, (B) presenting the morphology of the reported nano/microrobots employed for treatment of stomach diseases and imaging. (C) Presenting the means used to propel nano/microrobots in the treatment of stomach diseases.

## 2. Nano/Microrobots (NMR) in Action for Stomach Diseases

### 2.1. Zinc (Zn)-Based NMRs

Wang et al. [31] reported the first in vivo study of synthetic Zn-based microrobots using a live mouse model. Microrobots were fabricated using the electrochemical deposition method using Cyclopore polycarbonate membrane templates (**Figure 1A**). PEDOT/Zn microrobots were prepared as follows: (I) deposition of the poly (3,4-ethylenedioxythiophene (PEDOT) microtube, (II) deposition of the inner zinc layer, and (III) dissolution of the membrane and release of the microrobots. The resulting PEDOT/Zn microrobots were able to swim autonomously in the simulated gastric fluid (pH = 1.2) as Zn participated in a redox reaction, oxidized, and ejected H<sub>2</sub> bubbles (~60  $\mu\text{ms}^{-1}$ ). Their retention properties were examined using a mouse model. In this regard, PEDOT/Zn microrobots are compared with PEDOT/Platinum (Pt) microrobots (they could not move in gastric juice). The results reveal that after two hours, a large number of PEDOT/Zn microrobots were observed on the stomach wall, while in the control experiment the retention of the PEDOT/Pt microrobots on the stomach wall was significantly lower. It was shown that the propulsion of Zn-based microrobots in the acid environment of the stomach facilitated their penetration and retention in the porous, gel-like mucus layer of the stomach wall. As time increased, the number of retained microrobots decreased due to their degradation and transfer to the small intestine (**Figure 1B**).

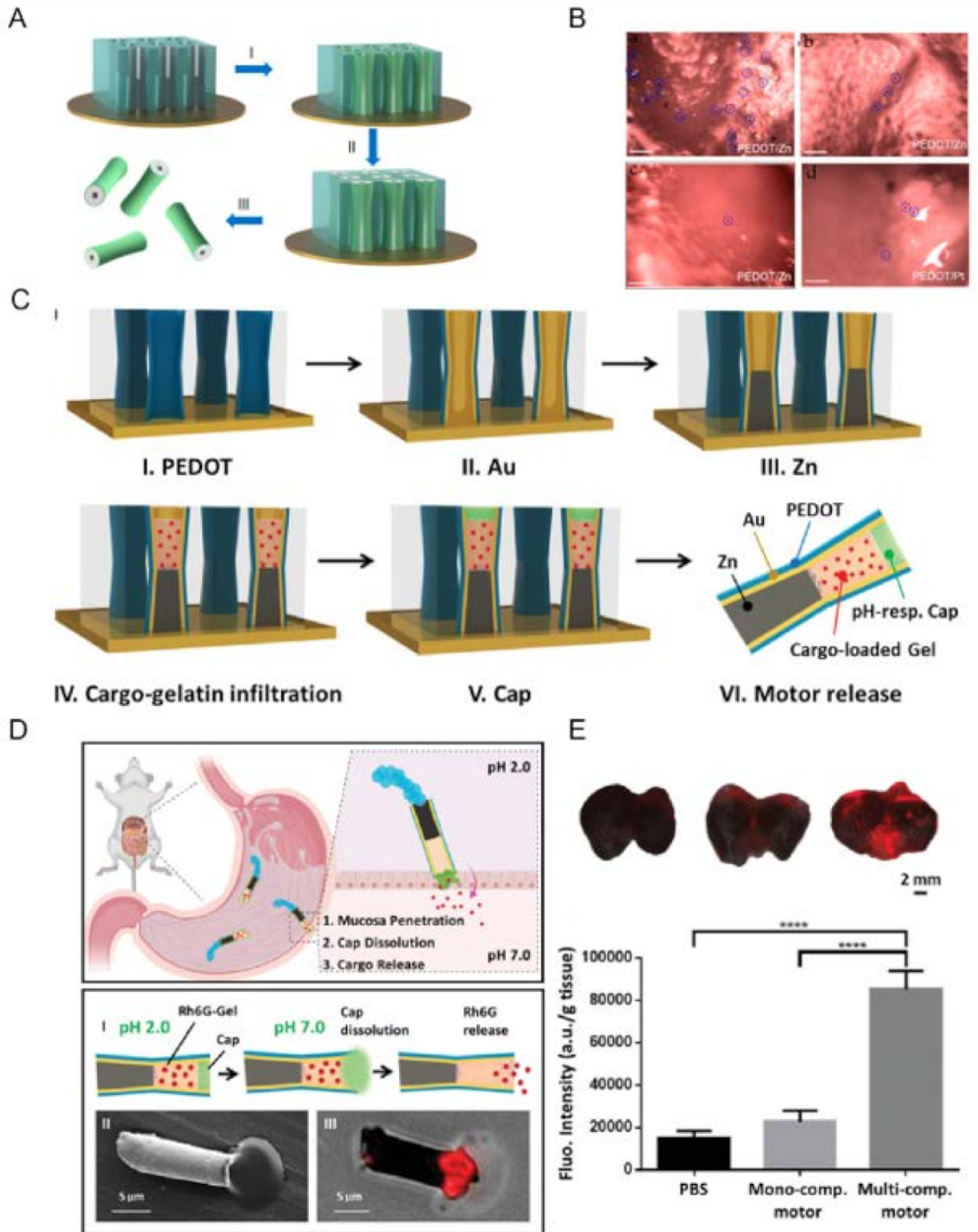


**Figure 1.** Zn-based NMRs. **(A)** Preparation of PEDOT/Zn microrobots: (I) deposition of the PEDOT microtube, (II) deposition of the inner zinc layer, and (III) dissolution of the membrane and release of the micromotors. **(B)** Microscopic images illustrate the retained micromotors in the stomach tissues collected at (a) 2 h, (b) 6 h, and (c) 12 h post-oral administration of PEDOT/Zn micromotors and (d) 2 h post-oral administration of PEDOT/Pt micromotors (serving as a negative control). Scale bars, 100  $\mu\text{m}$ . (Reproduced with permission from Ref. [31], Copyright © 2014 American Chemical Society.) **(C)** Schematic of the preparation of the multicompartiment motor: (I) PEDOT electropolymerization; (II) Au electrodeposition; (III) galvanostatic electrodeposition of Zn; (IV) cargo-loaded gelatin infiltration for 20 min at 50 °C; (V) protective cap using 8% Eudragit L100 polymer, and (VI) release of the multicompartiment motor by dissolving the polycarbonate membrane template. **(D)** Top panel: Schematic of the propulsion and distribution of the multicompartiment motors in a mouse stomach along with the efficient tissue penetration, dissolution of the enteric coating, and responsive release of the cargo in the gastric lining. Bottom panel: Schematic of the dissolution of the enteric cap, along with the release of the Rh6G cargo from the multicompartiment motor (I); SEM (II) and merged microscopy (III) images showing the release of the Rh6G-loaded gelatin from the multicompartiment motor. **(E)** Top (from left to right): merged images of the luminal lining of freshly excised mouse stomach at 2 h after oral gavage of PBS (control), monocompartiment motors and multicompartiment motors. Bottom: corresponding fluorescence quantification of the three groups. Error bars calculated as a triple of s.d. ( $n = 3$ ) (\*\*\*\*  $p < 0.0001$ ).

## 2.2. Magnesium (Mg)-Based NMRs

Magnesium-based NMRs are also similar to Zn-based robots. They can directly use their surrounding medium (aqueous) as fuel to produce  $\text{H}_2$  bubbles for swimming. These robots eliminate the need for commonly used toxic fuels. Mg-based microrobots have been designed in tubular and Janus shapes for the treatment of stomach diseases.

Wang et al. [32] reported a tubular PEDOT/Au robot used as a container to load Mg particles and the cargo model (Au NPs) inside (**Figure 2A**). The microrobots were covered with an enteric polymer as a protection layer against gastric juice. This polymeric layer is stable in an acid environment (pH 1–3) while it dissolves in neutral and alkaline media (pH 6–7), which allows robots to deliver cargo safely. The thickness of the polymeric layer can be tuned according to the time required for the travel of the robot through the gastrointestinal tract before its propulsion is activated. The results show that the dissolution of the polymer and the propulsion of the robots took around 10 min for a thin coating (0.3  $\mu\text{m}$ ), while for a medium (0.8  $\mu\text{m}$ ) and thick (1.2  $\mu\text{m}$ ) coating, the robot activation was much slower, 30–40 min and 3 h, respectively. Interestingly, for each thickness of the polymeric coating, activation occurred in different segments (upper, middle, and lower) of the gastrointestinal tract (GI). These results prove that, by controlling the coating thickness, the positioning of the robots can be selected in different regions of the GI. The functionality of these robots was examined in a mouse model (oral administration), and the in vivo results show that Mg-based microrobots swam securely through the gastric fluid and were activated in the GI tract. Like Zn-based robots, it was expected that the propulsion of Mg-based robots increases local retention and penetration because of their swimming and trapping in the mucus layer. In this regard, the PEDOT/Au robot loaded with the Mg was compared with silica microsphere-loaded (no propulsion). The results show that the fluorescence intensity of the



images of the pH indicator BCECF superimposed on the entire stomach for the 20 min and 24 h post-administration of 5 mg of the Mg micromotor. Mice treated with water were used as a control (reproduced with permission from Ref. [33], published by John Wiley and Sons, 2017) (C) Left panel (top): Schematic of micromotor pill dissolution in gastric fluid and subsequent micromotor release. Left panel (bottom): Bright-field, fluorescent (DiD dye loaded onto the micromotors), and merged images of the luminal lining of freshly excised mouse stomachs at 4 h after oral gavage of DI water (naïve), using DiD-loaded silica pills, free DiD-loaded Mg-based micromotors, or DiD-loaded Mg-based micromotor pills. Scale bar, 5 mm. Right panel: Schematic in vivo actuation of a micromotor pill (not to scale): pill dissolution in gastric fluid, micromotor release, and distribution of fluorescent cargoes in mouse stomach tissue (reproduced with permission from Ref. [34], Copyright © 2018 American Chemical Society). (D) Schematic of micromotor toxoids for oral vaccination. Top panel: Motor toxoids are fabricated by a sequential process in which magnesium (Mg) microparticles are coated with an asymmetrical layer of TiO<sub>2</sub>, followed by a toxin-inserted RBC membrane (RBC-toxin) as the antigenic material, mucoadhesive chitosan, and a pH-sensitive enteric coating. Bottom panel: When administered orally to mice, motor toxoids first enter the stomach, where the enteric coating protects the formulation from degradation in the low pH environment. With the more neutral pH of the intestine, the enteric coating dissolves and the intestinal fluid activates the motors. The autonomous propulsion of the motors enables enhanced retention and penetration in the intestinal wall, enhancing immune stimulation against the antigenic payload (reproduced with permission from Ref. [35], Copyright © 2019 American Chemical Society). (E) Left panel: Schematic of PAMR in vivo. (i) Schematic of the PAMR in the GI tract. The MCs are administered to the mouse. NIR illumination facilitates the real-time PA imaging of the MCs and subsequently triggers the propulsion of the micromotors in targeted areas of the GI tract. (ii) Schematic of PACT of the MCs in the GI tract in vivo. The mouse was kept in the water tank surrounded by an elevational focused ultrasound transducer array. NIR side illumination onto the mouse generated PA signals, which were subsequently received by the transducer array. (Inset) Enlarged view of the yellow dashed box region, illustrating the confocal design of light delivery and PA detection. US, ultrasound; CL, conical lens; DAQ, data acquisition system. (iii) Enteric coating prevents the decomposition of MCs in the stomach. (iv) External CW NIR irradiation induced the phase transition and subsequent collapse of the MCs on demand in the targeted areas and activated the movement of the micromotors upon unwrapping from the capsule. (v) Active propulsion of the micromotors promoted retention and cargo delivery efficiency in intestines. Middle panel (top and bottom): The stability of the MCs in gastric acid and intestinal fluid (top) without CW NIR irradiation and the use of CW NIR irradiation to trigger the collapse of an MC and the activation of the micromotors (bottom). Right panel: Time-lapse PACT images of the MCs in intestines for 7.5 h. The MCs migrating in the intestine are shown in color; the mouse tissues are shown in gray. Scale bar, 2 mm.

The resulting microrobots are covered by a red blood cell (RBC) membrane loaded with Staphylococcal  $\alpha$ -toxin as a cargo model. The robots were then coated with chitosan, which was negatively charged to provide electrostatic interaction. Finally, the microrobot is packed in an enteric polymer, Eudragit L100–55, to protect the robot against acidic conditions (Figure 2D). Therefore, as previously mentioned, these robots can safely pass through the stomach and reach the intestine. The intestine environment is neutral, which can facilitate the dissolution of the polymeric layer and the activation of robots. They explored the interaction between the introduced microrobots and

live cells and compared the result with static particles (without movement). The higher uptake of cells by active robots confirmed that propulsion enhances cell interaction. Finally, they evaluated the potency of the robot-based vaccine using a mouse model. One week after administration (orally), the antibody test was performed. The results reveal that the antitoxin IgA increased significantly, which shows that NMR technology helps deliver and retain antigenic payloads (**Figure 2D**).

However, as mentioned above, researchers have put much effort into the development of NMRs, imaging, positioning, and monitoring of NMR propulsion still remain the main challenges for biomedical in vivo application. In biomedical applications, optical imaging is a common tool, but difficulties arise when it is used for deep tissues. Due to light scattering, the image resolution drops significantly, which limits its application. In this regard, photoacoustic tomography (PAT) suggests deep tissue penetration, high resolution, and molecular contrast. Wu et al. [36] developed photoacoustic computed tomography-guided microrobots for gastrointestinal therapy.

Microrobots based on Mg were manufactured as previously reported (**Figure 2E**, left panel). The microrobots were then encapsulated in enteric polymer to survive in the acidic environment of the stomach and passed to the intestines to propel and release the cargo. In the design of the microrobot, an Au layer was employed to increase light absorption for photoacoustic imaging. Therapeutic drugs and imaging agents were embedded in a hydrogel layer to provide maximum capacity. Microcapsules (encapsulated microrobots) can be activated using continuous-wave Near-infrared (NIR). The Au layer converts NIR light to heat, causing the release of microrobots from the capsule. This photothermal effect not only releases the microrobots but also accelerates the Mg–water reaction that results in higher speed propulsion (**Figure 2E**, middle panel). The function of the designed microrobots was examined using a mouse model for in vivo application. The Mg-based microrobot coated with enteric polymer was administered orally to the mouse. Twelve hours after administration, the retention of the Mg-based microrobot in the GI was evaluated. A much higher number of microrobots was retained compared with the passive particles. In the targeted drug delivery application (colon cancer), doxorubicin-loaded microrobots showed a higher release rate compared to capsules loaded with doxorubicin alone (**Figure 2E**, right panel).

### 2.3. CaO<sub>2</sub>/Pt NPs Powered NMRs

Later, the research group of Zhang and Han introduced silica nanobottles (Si NBs) with a hydrophobic outer surface and a hydrophilic inner as a novel concept [37]. The hollow structure of Si NBs provides an efficient drug loading capacity. Clarithromycin (CLA), nano CaO<sub>2</sub>, and Pt NPs were loaded into Si NBs through amphiphilic interaction (**Figure 3(Aa,b)**). Upon delivery of the nanorobots to the stomach area, CaO<sub>2</sub> can react with gastric juice, consume protons, and produce hydrogen peroxide. The produced H<sub>2</sub>O<sub>2</sub> could react with Pt NPs and drive the Si NB robots (**Figure 3(Ac,d)**). As Si NB robots propel in acid media by consuming the proton, the environment becomes neutral (**Figure 3(Bi)**). The cargo could be also released by ejecting bubbles due to the reaction between Pt NPs and produced H<sub>2</sub>O<sub>2</sub>. Si NBs were administered orally to mice for five consecutive days and the in vivo toxicity profile was evaluated according to changes in body weight. The results confirm that there were no significant differences. In addition to body weight, blood biochemical analysis, gastrointestinal histopathology, and internal organ pathology have been performed to confirm the biosafety of the CLA/CaO<sub>2</sub>/Pt@Si NB robots. The

potential medical application of Si NBs for the treatment of *H. pylori* infection was examined using mouse models. The result of treatment with CLA/CaO<sub>2</sub>/Pt@Si NB was compared with common oral treatment (PPI + CLA) and revealed that there were no significant differences between the two groups in terms of treatment; however, PPI was observed to cause severe damage to gastric cells. Interestingly, in the case of the stomach pH value of CLA/CaO<sub>2</sub>/Pt@Si NB, the pH value returned to normal shortly, while for the group treated with PPI, this reverse was difficult. This could be the result of damage to gastric tissue cells caused by PPI (**Figure 3**(Bii–vi)).

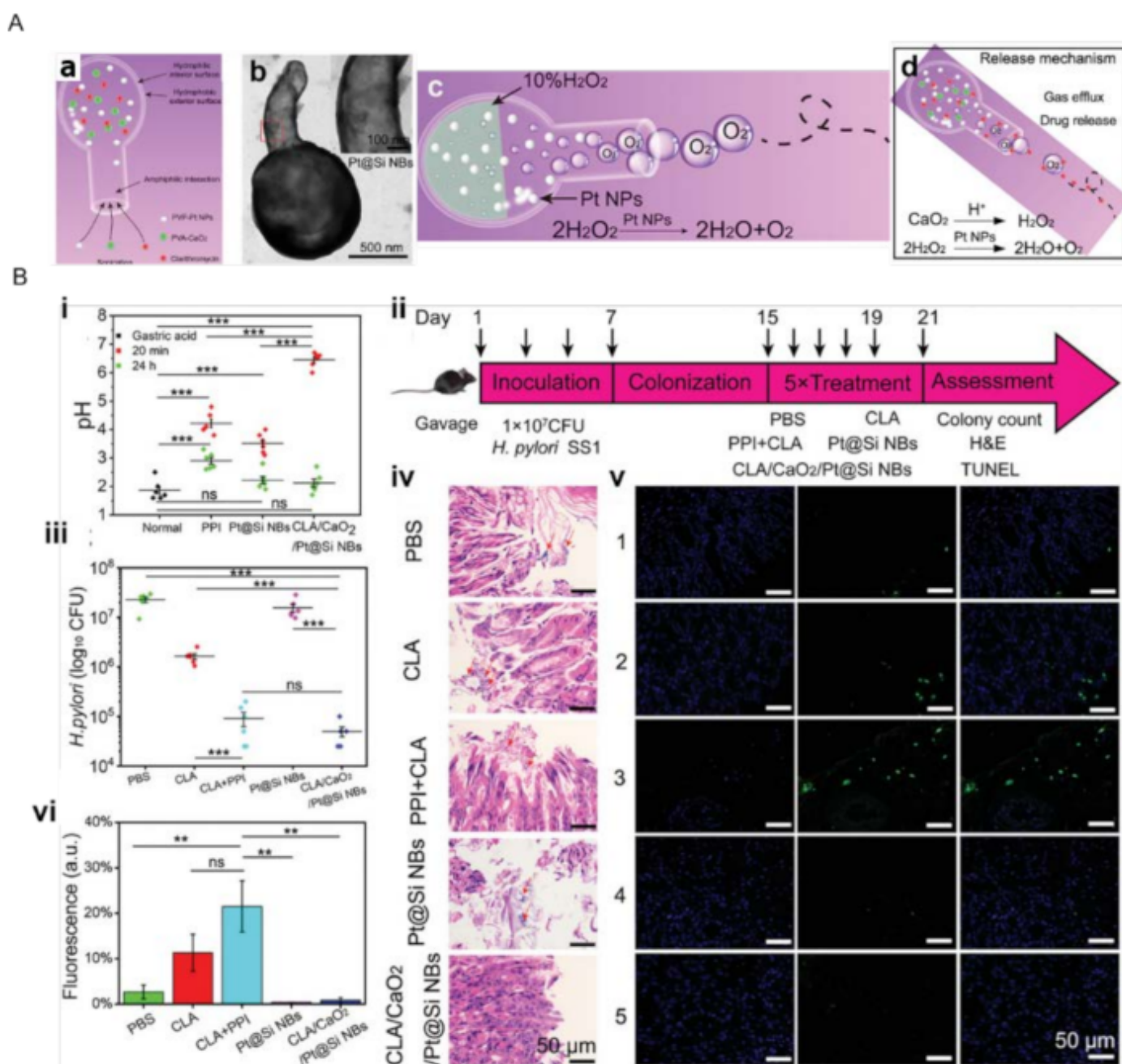


**Figure 3.** (A): (a) Selective loading of hydrophilic NPs on the interior surface of Si NBs. (b) TEM imaging of Pt@Si NBs. (c) Schematic diagram of the nanomotor driving mechanism. (d) Release mechanism of CLA. (B): *H. pylori*-infected treatment in vivo. (i) pH neutralization process at 20 min (red) and 24 h (green) after oral 400 μmol kg<sup>-1</sup> PPI, 15 mg Pt@Si NBs, and 15 mg CLA/CaO<sub>2</sub>/Pt@Si NBs. (ii) Animal model treatment experiment process. (iii)

Number of *H. pylori* in gastric tissue after different treatments. (iv) H&E staining and (v) the TUNEL staining of the stomach after different treatment (1. PBS, 2. CLA, 3. PPI + CLA, 4. Pt@Si NBs, 5. CLA/CaO<sub>2</sub>/Pt@Si NBs). (vi) Quantitative evaluation of TUNEL staining (\*\*  $p < 0.01$ , \*\*\*  $p < 0.001$ , ns, not significant).

## 2.4. Enzyme-Powered NMRs

Although Mg- and Zn-based NMRs have been successful in the treatment of GI diseases, there are still some challenges, such as their fuels and biodegradability. As the Mg/Zn catalytic reaction with the surrounding environment is aggressive, there is a potential for tissue damage. Another concern was raised about the retention of nondegradable residues in the stomach wall. For the treatment of stomach diseases, robot actuation is crucial. Therefore, alternative options are magnetized [7] or enzyme-based [5][38][39][40] NMRs with biocompatible reactions and complete biodegradability. Hahn et al. [41] developed bioinspired polydopamine (PDA) microrobots that used urea in the stomach as a biofuel for propulsion (Figure 4A,B). The silica microparticle was first covered by PDA polymerization, then the silica core was dissolved in HF solution, and the hollow polydopamine particles were placed in urease solution for immobilization via a Schiff base reaction. These microrobots hydrolyze urea using their conjugated urease and form ammonia and CO<sub>2</sub>. This propulsion facilitated the robot's penetration to the stomach wall. The in vivo experiment (mice model) showed a remarkable improvement in penetration and prolonged retention in the stomach for one day. The microrobots disappeared after 3 days without causing any gastrointestinal tract toxicity (Figure 4C,D). This work demonstrated the feasibility of the potential use of stomach disease treatment using bioinspired and biodegradable microrobots [41].

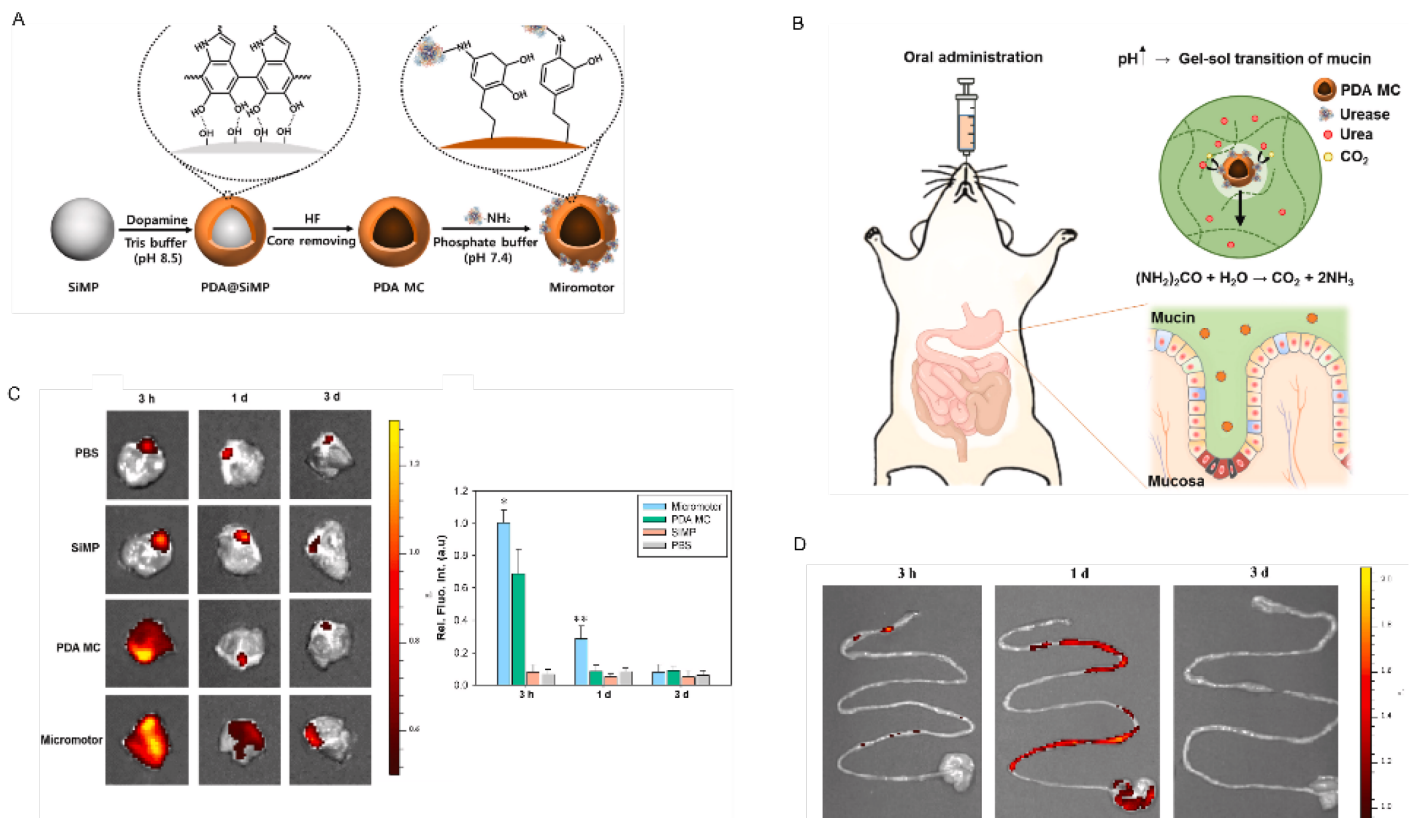


**Figure 4.** Schematic illustration for (A) the preparation procedure of urease-powered micromotors using silica microparticle (SiMP) and polydopamine microcapsule (PDA MC), and (B) the oral delivery of urease-powered polydopamine micromotors for enhanced penetration and retention in the stomach. (C) Left panel: IVIS images of the intact stomach at 3 h, 1 d and 3 d post-oral injection of PBS, SiMP, PDA MC and micromotors and right panel: the corresponding quantified fluorescence intensity at each time point ( $n = 3$ ). (D) IVIS images of the intestinal tract at 3 h, 1 d, and 3 d post-oral administration of micromotors. (\*  $p \leq 0.05$ , \*\*  $p \leq 0.01$ , micromotor vs. PDA MC).

## 2.5. Biohybrid NMRs

As mentioned above, one of the main challenges in NMR design is its biocompatibility. One of the solutions is to explore the nature database for biological units with inherited functionalities that can be employed in the design and engineering of the NMRs. The use of microorganisms such as sperm, neutrophils, algae, and bacteria in NMR design has been explored and promising results have been achieved [42][43]. Microalgae organisms have drawn much attention in the biomedical field as novel biological materials with inherent characteristics such as autofluorescent pigments, magnetic resonance signals, biodegradability, and low cytotoxicity [44][45]. Zhang et al. developed a microrobot based on *Spirulina platensis* (helical shapes) for active targeted delivery and imaging purposes in vivo [46][47]. They covered *Spirulina platensis* with  $\text{Fe}_3\text{O}_4$  nanoparticles through a simple dip-coating process (Figure 5A). Integrating the  $\text{Fe}_3\text{O}_4$  NPs into *Spirulina platensis* equipped them for remote actuation using an external magnetic field. They were able to swim in different media including DI water, blood, gastric juice, urine, and even peanut oil. As mentioned earlier, *Spirulina platensis* has instinct fluorescence, making it an ideal biomarker in biomedical applications. In this regard, their fluorescence stability was tested and the results reveal that over 60 min of illumination, the fluorescence was still stable, without any significant bleaching. Furthermore, the fluorescence signal was evaluated in different media such as neutral, alkaline, and acidic solutions, physiological media (containing 5% dextrose and phosphate-buffered saline), cell growth media, and isopropyl alcohol. The signal weakened only in acidic solution and IPA, while it remained without significant changes in the rest. The introduced microrobots have been used for in vivo imaging in (a) right below the dermis and (b) space between the parietal peritoneum and the visceral peritoneum of nude mice (Figure 5B). The results show that different factors contributed to the fluorescence signal, including (i) fluorescence characteristics, (ii) magnetization property, and (iii) an in situ environment. However, fluorescence-based biomedical imaging is a great help for the in vivo positioning of NMRs; it cannot penetrate deep tissues (more than few centimeters), which limits its application. One of the promising methods for deep tissues is magnetic resonance imaging (MRI), as *Spirulina platensis* covered with  $\text{Fe}_3\text{O}_4$  NPs can function as MR imaging contrast agents. The observed images revealed that the intensity of the contrast is a function of two factors: (a) concentration and (b) magnetization time. By prolonging the magnetization time, the imaging contrast could be significantly increased. The *Spirulina platensis* robots were tested for in vivo MR imaging in deep tissue (i.e., stomach) using a mouse model (Figure 5C). The results of the two different doses (4 mg/mL and 8 mg/mL) reveal that the MR contrasts depend on the concentration (4 mg/mL < 8 mg/mL).

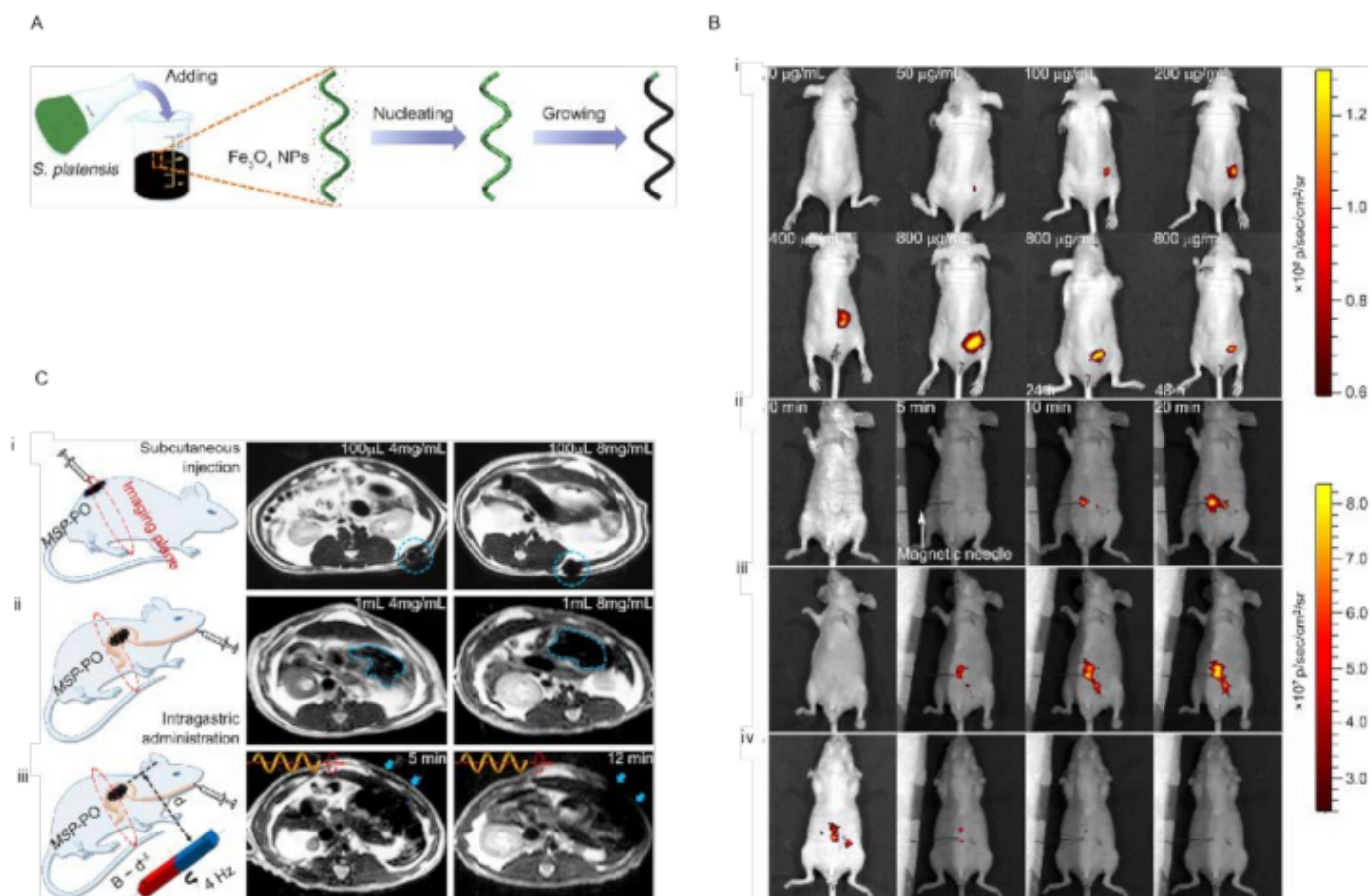


**Figure 5.** (A) Schematic of the dip-coating process of *S. platensis* in a suspension of  $\text{Fe}_3\text{O}_4$  NPs. (B) (i) Fluorescence of 100  $\mu\text{L}$  of MSP-72h with varying concentrations in the subcutaneous tissue of nude Balb/c athymic mice at three residence times. The residence time is 0 min unless otherwise specified. Fluorescence of 300  $\mu\text{L}$  of (ii) MSP-72h, (iii) MSP-24h, and (iv) MSP-6h (all 800  $\mu\text{g}/\text{mL}$ ) in the intraperitoneal cavity at various residence times. Image sequences of (iii) and (iv) were recorded at the same time intervals with (ii). The magnetic needle was placed at  $t = 3$  min. (C) (i) MSP swarm of two different concentrations inside the subcutaneous tissues. (ii) MSP swarm of two different concentrations inside the stomach. (iii) MSP swarm with the same concentration but subject to actuation and steering (with a rotating magnetic field) for different time periods before MR imaging across the rat's stomach.

## References

1. Fleischer, R. *Fantastic Voyage*; 20th Century Fox: Los Angeles, CA, USA, 1966.
2. Feynman, R.P. There's plenty of room at the bottom. *Resonance* 2011, 16, 890.
3. Paxton, W.F.; Kistler, K.C.; Olmeda, C.C.; Sen, A.; St. Angelo, S.K.; Cao, Y.; Mallouk, T.E.; Lammert, P.E.; Crespi, V.H. Catalytic Nanomotors: Autonomous Movement of Striped Nanorods. *J. Am. Chem. Soc.* 2004, 126, 13424–13431.

4. Arqué, X.; Romero-Rivera, A.; Feixas, F.; Patiño, T.; Osuna, S.; Sánchez, S. Intrinsic enzymatic properties modulate the self-propulsion of micromotors. *Nat. Commun.* 2019, 10, 2826.
5. Dey, K.K.; Zhao, X.; Tansi, B.M.; Méndez-Ortiz, W.J.; Córdova-Figueroa, U.M.; Golestanian, R.; Sen, A. Micromotors Powered by Enzyme Catalysis. *Nano Lett.* 2015, 15, 8311–8315.
6. Chen, C.; Karshalev, E.; Guan, J.; Wang, J. Magnesium-Based Micromotors: Water-Powered Propulsion, Multifunctionality, and Biomedical and Environmental Applications. *Small* 2018, 14, 1704252.
7. Koleoso, M.; Feng, X.; Xue, Y.; Li, Q.; Munshi, T.; Chen, X. Micro/nanoscale magnetic robots for biomedical applications. *Mater. Today Bio* 2020, 8, 100085.
8. Lee, J.G.; Al Harraq, A.; Bishop, K.J.M.; Bharti, B. Fabrication and Electric Field-Driven Active Propulsion of Patchy Microellipsoids. *J. Phys. Chem. B* 2021, 125, 4232–4240.
9. Lu, X.; Shen, H.; Zhao, K.; Wang, Z.; Peng, H.; Liu, W. Micro-/Nanomachines Driven by Ultrasonic Power Sources. *Chem. Asian J.* 2019, 14, 2406–2416.
10. Bunea, A.-I.; Martella, D.; Nocentini, S.; Parmeggiani, C.; Taboryski, R.; Wiersma, D.S. Light-Powered Microrobots: Challenges and Opportunities for Hard and Soft Responsive Microswimmers. *Adv. Intell. Syst.* 2021, 3, 2000256.
11. Wan, M.; Li, T.; Chen, H.; Mao, C.; Shen, J. Biosafety, Functionalities, and Applications of Biomedical Micro/nanomotors. *Angew. Chem. Int. Ed.* 2021, 60, 13158–13176.
12. Li, M.; Xi, N.; Wang, Y.; Liu, L. Progress in Nanorobotics for Advancing Biomedicine. *IEEE Trans. Biomed. Eng.* 2021, 68, 130–147.
13. Parmar, J.; Vilela, D.; Villa, K.; Wang, J.; Sánchez, S. Micro- and Nanomotors as Active Environmental Microcleaners and Sensors. *J. Am. Chem. Soc.* 2018, 140, 9317–9331.
14. Singh, V.V.; Wang, J. Nano/micromotors for security/defense applications. A review. *Nanoscale* 2015, 7, 19377–19389.
15. Molinero-Fernández, Á.; Jodra, A.; Moreno-Guzmán, M.; López, M.Á.; Escarpa, A. Magnetic Reduced Graphene Oxide/Nickel/Platinum Nanoparticles Micromotors for Mycotoxin Analysis. *Chem. Eur. J.* 2018, 24, 7172–7176.
16. Bulatov, E.; Khaiboullina, S.; dos Reis, H.J.; Palotás, A.; Venkataraman, K.; Vijayalakshmi, M.; Rizvanov, A. Ubiquitin-Proteasome System: Promising Therapeutic Targets in Autoimmune and Neurodegenerative Diseases. *BioNanoScience* 2016, 6, 341–344.
17. Lin, R.; Yu, W.; Chen, X.; Gao, H. Self-Propelled Micro/Nanomotors for Tumor Targeting Delivery and Therapy. *Adv. Healthc. Mater.* 2021, 10, 2001212.

18. Sun, M.; Fan, X.; Meng, X.; Song, J.; Chen, W.; Sun, L.; Xie, H. Magnetic biohybrid micromotors with high maneuverability for efficient drug loading and targeted drug delivery. *Nanoscale* 2019, 11, 18382–18392.
19. Srivastava, S.K.; Clergeaud, G.; Andresen, T.L.; Boisen, A. Micromotors for drug delivery in vivo: The road ahead. *Adv. Drug Deliv. Rev.* 2019, 138, 41–55.
20. Xu, H.; Medina-Sánchez, M.; Magdanz, V.; Schwarz, L.; Hebenstreit, F.; Schmidt, O.G. Sperm-Hybrid Micromotor for Targeted Drug Delivery. *ACS Nano* 2018, 12, 327–337.
21. Luo, M.; Feng, Y.; Wang, T.; Guan, J. Micro-/Nanorobots at Work in Active Drug Delivery. *Adv. Funct. Mater.* 2018, 28, 1706100.
22. Blaser, M.J. *Helicobacter pylori* and the pathogenesis of gastroduodenal inflammation. *J. Infect. Dis.* 1990, 161, 626–633.
23. Rotimt, O.; Nduduba, D.A.; Otegbeye, F.M. *Helicobacter pylori* and the pathogenesis of gastroduodenal disease: Implications for the management of peptic ulcer disease. *Niger. Postgrad. Med. J.* 2005, 12, 289–298.
24. Asaka, M.; Sugiyama, T.; Kato, M.; Satoh, K.; Kuwayama, H.; Fukuda, Y.; Fujioka, T.; Takemoto, T.; Kimura, K.; Shimoyama, T.; et al. A multicenter, double-blind study on triple therapy with lansoprazole, amoxicillin and clarithromycin for eradication of *Helicobacter pylori* in Japanese peptic ulcer patients. *Helicobacter* 2001, 6, 254–261.
25. Tsay, F.-W.; Hsu, P.-I.H. *pylori* infection and extra-gastroduodenal diseases. *J. Biomed. Sci.* 2018, 25, 65.
26. Sugiyama, A.; Maruta, F.; Ikeno, T.; Ishida, K.; Kawasaki, S.; Katsuyama, T.; Shimizu, N.; Tatematsu, M. *Helicobacter pylori* infection enhances N-methyl-N-nitrosourea-induced stomach carcinogenesis in the Mongolian gerbil. *Cancer Res.* 1998, 58, 2067–2069.
27. Kalisperati, P.; Spanou, E.; Pateras, I.S.; Korkolopoulou, P.; Varvarigou, A.; Karavokyros, I.; Gorgoulis, V.G.; Vlachoyiannopoulos, P.G.; Sougioultzis, S. Inflammation, DNA Damage, *Helicobacter pylori* and Gastric Tumorigenesis. *Front. Genet.* 2017, 8, 20.
28. Jaynes, M.; Kumar, A.B. The risks of long-term use of proton pump inhibitors: A critical review. *Ther. Adv. Drug Saf.* 2018, 10, 2042098618809927.
29. Debraekeleer, A.; Remaut, H. Future perspective for potential *Helicobacter pylori* eradication therapies. *Future Microbiol.* 2018, 13, 671–687.
30. De Ávila, B.E.-F.; Angsantikul, P.; Li, J.; Angel Lopez-Ramirez, M.; Ramírez-Herrera, D.E.; Thamphiwatana, S.; Chen, C.; Delezuk, J.; Samakapiruk, R.; Ramez, V.; et al. Micromotor-enabled active drug delivery for in vivo treatment of stomach infection. *Nat. Commun.* 2017, 8, 272.

31. Gao, W.; Dong, R.; Thamphiwatana, S.; Li, J.; Gao, W.; Zhang, L.; Wang, J. Artificial Micromotors in the Mouse's Stomach: A Step toward in Vivo Use of Synthetic Motors. *ACS Nano* 2015, 9, 117–123.
32. Li, J.; Thamphiwatana, S.; Liu, W.; Esteban-Fernández de Ávila, B.; Angsantikul, P.; Sandraz, E.; Wang, J.; Xu, T.; Soto, F.; Ramez, V.; et al. Enteric Micromotor Can Selectively Position and Spontaneously Propel in the Gastrointestinal Tract. *ACS Nano* 2016, 10, 9536–9542.
33. Li, J.; Angsantikul, P.; Liu, W.; Esteban-Fernández de Ávila, B.; Thamphiwatana, S.; Xu, M.; Sandraz, E.; Wang, X.; Delezuk, J.; Gao, W.; et al. Micromotors Spontaneously Neutralize Gastric Acid for pH-Responsive Payload Release. *Angew. Chem. Int. Ed.* 2017, 56, 2156–2161.
34. Karshalev, E.; Esteban-Fernández de Ávila, B.; Beltrán-Gastélum, M.; Angsantikul, P.; Tang, S.; Mundaca-Urbe, R.; Zhang, F.; Zhao, J.; Zhang, L.; Wang, J. Micromotor Pills as a Dynamic Oral Delivery Platform. *ACS Nano* 2018, 12, 8397–8405.
35. Wei, X.; Beltrán-Gastélum, M.; Karshalev, E.; Esteban-Fernández de Ávila, B.; Zhou, J.; Ran, D.; Angsantikul, P.; Fang, R.H.; Wang, J.; Zhang, L. Biomimetic Micromotor Enables Active Delivery of Antigens for Oral Vaccination. *Nano Lett.* 2019, 19, 1914–1921.
36. Wu, Z.; Li, L.; Yang, Y.; Hu, P.; Li, Y.; Yang, S.-Y.; Wang, L.V.; Gao, W. A microrobotic system guided by photoacoustic computed tomography for targeted navigation in intestines in vivo. *Sci. Robot.* 2019, 4, eaax0613.
37. Wu, Y.; Song, Z.; Deng, G.; Jiang, K.; Wang, H.; Zhang, X.; Han, H. Gastric Acid Powered Nanomotors Release Antibiotics for In Vivo Treatment of *Helicobacter pylori* Infection. *Small* 2021, 17, 2006877.
38. Yuan, H.; Liu, X.; Wang, L.; Ma, X. Fundamentals and applications of enzyme powered micro/nano-motors. *Bioact. Mater.* 2021, 6, 1727–1749.
39. Patiño, T.; Arqué, X.; Mestre, R.; Palacios, L.; Sánchez, S. Fundamental Aspects of Enzyme-Powered Micro- and Nanoswimmers. *Acc. Chem. Res.* 2018, 51, 2662–2671.
40. Mathesh, M.; Sun, J.; Wilson, D.A. Enzyme catalysis powered micro/nanomotors for biomedical applications. *J. Mater. Chem. B* 2020, 8, 7319–7334.
41. Choi, H.; Jeong, S.H.; Kim, T.Y.; Yi, J.; Hahn, S.K. Bioinspired urease-powered micromotor as an active oral drug delivery carrier in stomach. *Bioact. Mater.* 2021, 9, 54–62.
42. Alapan, Y.; Yasa, O.; Yigit, B.; Yasa, I.C.; Erkoc, P.; Sitti, M. Microrobotics and Microorganisms: Biohybrid Autonomous Cellular Robots. *Annu. Rev. Control Robot. Auton. Syst.* 2019, 2, 205–230.
43. Lin, Z.; Jiang, T.; Shang, J. The emerging technology of biohybrid micro-robots: A review. *Bio-Des. Manuf.* 2021. Available online: <https://link.springer.com/article/10.1007/s42242-021-00135-6#citeas> (accessed on 16 May 2021).

44. Zhong, D.; Du, Z.; Zhou, M. Algae: A natural active material for biomedical applications. *VIEW* 2021. Available online: <https://onlinelibrary.wiley.com/doi/full/10.1002/VIW.20200189> (accessed on 23 February 2021).
45. Wang, H.-D.; Li, X.-C.; Lee, D.-J.; Chang, J.-S. Potential biomedical applications of marine algae. *Bioresour. Technol.* 2017, 244, 1407–1415.
46. Yan, X.; Zhou, Q.; Vincent, M.; Deng, Y.; Yu, J.; Xu, J.; Xu, T.; Tang, T.; Bian, L.; Wang, Y.-X.J.; et al. Multifunctional biohybrid magnetite microrobots for imaging-guided therapy. *Sci. Robot.* 2017, 2, eaaq1155.
47. Yan, X.; Zhou, Q.; Yu, J.; Xu, T.; Deng, Y.; Tang, T.; Feng, Q.; Bian, L.; Zhang, Y.; Ferreira, A.; et al. Magnetite Nanostructured Porous Hollow Helical Microswimmers for Targeted Delivery. *Adv. Funct. Mater.* 2015, 25, 5333–5342.

---

Retrieved from <https://encyclopedia.pub/entry/history/show/43962>